

Automated 3-Dimensional Elastic Registration of Whole-Body PET and CT from Separate or Combined Scanners

Raj Shekhar, PhD¹; Vivek Walimbe, BE^{2,3}; Shanker Raja, MD⁴; Vladimir Zagrodsky, PhD²; Mangesh Kanvinde, MD, PhD⁵; Guiyun Wu, MD⁶; and Bohdan Bybel, MD⁶

¹Department of Diagnostic Radiology, University of Maryland, Baltimore, Maryland; ²Department of Biomedical Engineering, Lerner Research Institute, The Cleveland Clinic Foundation, Cleveland, Ohio; ³Biomedical Engineering Center, The Ohio State University, Columbus, Ohio; ⁴Department of Radiology, Lahey Clinic, Burlington, Massachusetts; ⁵Department of Radiology, Medina General Hospital, Medina, Ohio; and ⁶Department of Molecular and Functional Imaging, The Cleveland Clinic Foundation, Cleveland, Ohio

Registration and fusion of whole-body functional PET and anatomic CT is significant for accurate differentiation of viable tumors from benign masses, radiotherapy planning and monitoring treatment response, and cancer staging. Whole-body PET and CT acquired on separate scanners are misregistered because of differences in patient positions and orientations, couch shapes, and breathing protocols. Although a combined PET/CT scanner removes many of these misalignments, breathing-related nonrigid mismatches still persist. **Methods:** We have developed a new, fully automated normalized mutual information-based 3-dimensional elastic image registration technique that can accurately align whole-body PET and CT images acquired on stand-alone scanners as well as a combined PET/CT scanner. The algorithm morphs the PET image to align spatially with the CT image by generating an elastic transformation field by interpolating quaternions and translations from multiple 6-parameter rigid-body registrations, each obtained for hierarchically subdivided image subvolumes. Fifteen whole-body (spanning thorax and abdomen) PET/CT image pairs acquired separately and 5 image pairs acquired on a combined scanner were registered. The cases were selected on the basis of the availability of both CT and PET images, without any other screening criteria, such as a specific clinical condition or prognosis. A rigorous quantitative validation was performed by evaluating algorithm performance in the context of variability among 3 clinical experts in the identification of up to 32 homologous anatomic landmarks. **Results:** The average execution time was 75 and 45 min for images acquired using separate scanners and combined scanner, respectively. Visual inspection indicated improved matching of homologous structures in all cases. The mean registration accuracy (5.5 and 5.9 mm for images from separate scanners and combined scanner, respectively) was found comparable to the mean interexpert difference in landmark identification (5.6 ± 2.4 and 6.6 ± 3.4 mm, respectively). The variability in landmark identification did not show statistically significant changes on replacing any expert by the algo-

rithm. **Conclusion:** We have presented a new and automated elastic registration algorithm to correct for nonrigid misalignments in whole-body PET/CT images as well as improve the "mechanical" registration of a combined PET/CT scanner. The algorithm performance was on par with the average opinion of 3 experts.

Key Words: image registration; elastic registration; whole-body PET/CT; multimodality; image fusion

J Nucl Med 2005; 46:1488–1496

Multimodality image fusion of whole-body PET and CT is clinically significant in that it permits an accurate localization of viable tumors, shown unequivocally by PET, with respect to the detailed anatomic map provided by CT (1–3). The information thus obtained is important for making a definitive diagnosis. Furthermore, the precise identification and localization of viable tumors with respect to CT are playing an increasing role in radiotherapy for the delivery of highly conformal doses to the tumor (4), monitoring treatment response, and recalibrating a treatment plan to focus progressively on the viable portion of the original tumor volume and spare treated and healthy tissues (5). Yet another use of fused PET/CT images is in cancer staging and the detection of recurrent tumors (4,6). The rapid emergence of combined PET/CT scanners in recent years is a confirmation of the clinical value, as well as the excitement, of merging complementary information from these 2 modalities.

Registration (alignment) of whole-body PET and CT images is a prerequisite for their meaningful fusion. Before the advent of combined PET/CT scanners, this registration could only be performed manually or using software methods. The manual approach is slow and tedious and generally corrects for rigid misalignment only. For higher accuracy, software methods implementing elastic image registration have been reported (6–8). Combined PET/CT scanners, on

Received Jan. 20, 2005; revision accepted May 6, 2005.

For correspondence or reprints contact: Raj Shekhar, PhD, Department of Diagnostic Radiology, University of Maryland School of Medicine, 22 S. Greene St., Baltimore, MD 21201.

E-mail: rshekhar@umm.edu

the other hand, perform image registration “mechanically” by performing the 2 scans successively while minimizing patient movement through the use of a common couch and then appropriately “sliding” one scan with respect to another.

The combined PET/CT scanners have undoubtedly simplified multimodality image registration and fusion. They have even sped up the overall scan time up to 40% (3) using the CT scan for PET attenuation correction. Nonetheless, the underlying registration mode remains rigid, which cannot compensate for involuntary nonrigid motion of thoracic and abdominal organs. Differences arise mainly due to varying breathing patterns. Whereas CT is generally performed with breath-hold or shallow breathing, longer PET scans are performed with the subject engaged in tidal breathing. The resulting misalignment in whole-body images is especially pronounced in the area of the diaphragm. In fact, up to 96% of combined PET/CT examinations have been reported to contain respiratory motion artifacts (9), with a target registration error as high as 11 mm (10). Developing and testing different breathing protocols to minimize motion artifacts in combined PET/CT images remain an area of active research (9–11). Therefore, despite the huge success of combined PET/CT scanners, it can be argued that the need for software-based (algorithmic) image registration persists and that its ability to correct for both rigid and nonrigid misalignments makes it applicable to whole-body CT and PET images, whether collected separately or on a combined scanner.

A software-based whole-body CT and PET image registration method must be automatic and fast and accommodate deformable anatomy to be clinically successful. These requirements, as we have argued before (12), rule out fiducial marker-based methods and make segmentation-based methods less desirable. Segmentation often requires manual intervention and can limit the overall accuracy of image registration. Even if it is automatic, the accuracy of nonrigid matching degrades away from the segmented features. For example, if the contour of the thorax is used for nonrigid registration of whole-body images as proposed by Slomka et al. (8), alignment of the abdominal features remains suspect. Voxel-based methods, especially those that maximize mutual information (MI) (13–15) or, its variant, normalized mutual information (NMI) (16), have emerged as the most accurate and robust measures (17,18) currently available for image registration. Because MI (or NMI) is a statistical measure that does not expect a direct correlation of intensities among homologous regions, it is a perfect measure for multimodality registration such as that between PET and CT. Successful application of multimodality MI/NMI-based image registration has been reported for many organs and imaging modalities (17,19–21). Our preliminary report (22), as well as works of others (8,23), demonstrates the potential of MI (or NMI) for whole-body elastic PET/CT registration.

We report here the development of a new fully automated algorithm for 3-dimensional (3D) elastic image registration. Following the description of the algorithm, we report its application to whole-body PET and CT images from separate as well as combined PET/CT scanners. We have used the opinion of 3 experts as a gold standard for validating the algorithm and found the algorithm’s performance on par with an expert’s ability to perform elastic registration using anatomic landmarks.

MATERIALS AND METHODS

Image Data

We report results of registration on a total of 20 clinically acquired whole-body PET/CT image pairs. Image data for all PET/CT registrations came from among the clinical cases archived at The Cleveland Clinic Foundation. The cases were picked by personnel, not familiar with the working of the registration algorithm, solely on the basis of availability of both CT and PET images, without any other screening criteria, such as a specific clinical condition or prognosis. After selection, it was determined that 6 cases showed the presence of a cancerous mass in the thoracic cavity as seen in CT or PET images. For each case, registration was performed using the higher-resolution CT image as the reference image and the attenuation-corrected PET emission scan as the floating image to be transformed to match the CT image.

Fifteen image pairs consisted of PET and CT acquired on separate scanners. Contrast-enhanced CT images were acquired (Somatom Plus; Siemens) with the subject involved in breath-holding at maximum inspiration and arms stretched over the head. The subject was involved in normal tidal breathing with arms beside the body during PET image acquisition (ECAT HR+; Siemens) lasting approximately 40–50 min. ^{18}F -FDG was injected as radiotracer about 45–60 min before scanning. Depending on the scanner settings (for optimum magnification of anatomy of clinical interest) at the time of image acquisition, CT images measured $512 \times 512 \times 70$ – 90 voxels with voxel dimensions in the range 0.9 – 1.2×0.9 – 1.2×5 mm. The typical image size for PET was $128 \times 128 \times 135$ – 160 voxels, with cubic voxels of dimensions $5.15 \times 5.15 \times 5.15$ mm. The attenuation-corrected PET emission scans, reflecting functional information for the entire body, generally had a larger field of view than the corresponding CT images. The time difference between acquisition of CT and PET images varied from a few minutes for some cases to a few days for others, dictated by clinical need, availability of equipment, and clinical scheduling issues at the time of acquisition.

We also performed registration of 5 cases consisting of PET and CT images acquired on a combined PET/CT scanner (Biograph Sensation 16; Siemens). During CT and PET image acquisition using the combined scanner, the subject was instructed to keep the arms beside the body and perform shallow breathing. ^{18}F -FDG was injected as the radiotracer about 45–60 min before scanning. At the time of scanning, the low-dose noncontrast-enhanced CT image was acquired first, followed by the PET image acquisition. No transmission PET scan was acquired, and the attenuation correction for PET was performed using the CT image. The typical image size for CT was $512 \times 512 \times 307$ – 404 voxels with a voxel size of $0.78 \times 0.78 \times 2.5$ mm, whereas the typical image size for

PET was $128 \times 128 \times 154$ – 202 voxels with a voxel size of $5.31 \times 5.31 \times 5$ mm.

To achieve a trade-off between maintaining CT resolution and obtaining nearly isotropic voxels, we resampled the CT images for all cases to get nearly isometric voxels with dimensions of 1.8 – 2.4×1.8 – 2.4×2.5 mm, depending on the original voxel dimensions. Resampling reduced the spatial resolution of CT images; however, the resulting images still had better spatial resolution than the PET images (the lower resolution image controls the accuracy of image registration in general) and nearly isotropic voxels. No preprocessing steps were used for the PET images.

Registration Algorithm

The algorithm is based on maximization of NMI and uses a hierarchical (pyramid) volume subdivision scheme to elastic image registration. Our algorithm initially recovers the global rigid-body mismatch between the reference (CT) and the floating (PET) image, followed by hierarchical refinement of the localized matching between the globally registered images. Initial development of the algorithm has been reported previously (22).

Global registration uses the 6-parameter rigid-body transformation model and is based on maximization of NMI between the 2 images. Next, we implement a hierarchical octree-based volume subdivision scheme. At each subdivision level, the floating image is registered with the individual subvolumes of the reference image, considered one at a time. Each subvolume registration continues until the iterative optimization process converges to a transformation solution (% NMI change < 0.1) or the maximum number of iterations (200) is reached. When all subvolume registrations at a given level are performed, the algorithm continues on to the next level of subdivision. Volume subdivision and subvolume registration continue until the voxel count for an individual subvolume remains above a predefined limit of 16^3 . This lower threshold was selected on the basis of the observation from pilot experiments for the given pair of modalities, which showed that over half the subvolume registrations with less than 16^3 voxels per subvolume failed to converge to a solution and thus did not significantly and robustly improve the existing alignment. Subvolume registration also uses a 6-parameter rigid-body transformation model. Initial seeding of the undivided floating image with respect to each subvolume is given by the transformation obtained from registration involving the floating image and the corresponding parent subvolume at the previous level of subdivision.

Subvolume registration is also based on maximization of NMI. During calculation of NMI for any given subvolume registration, we use the prior registration information for all remaining parts of the image, available from the previous hierarchical level. The prior information is assimilated into subvolume registration during calculation of NMI, by compiling the mutual histogram as a sum of 2 separate mutual histograms: $MH_{\text{subvolume}}$, calculated for the subvolume voxels, and MH_{prior} , calculated for all remaining voxels of the image, with transformations derived from the immediately preceding hierarchical level (22). The typical number of bins selected for the mutual histogram was 128×128 , based on calculations of optimal bin width as described (24). We implemented the steps in the NMI approach as outlined previously (16).

If the result of a given subvolume registration causes the effective subvolume displacement at that level above a preset threshold, we discard the solution and retain the transformation from the previous subdivision level. At each hierarchical level, this threshold is set equal to 25% of the smallest subvolume dimension at that

level. This provides a constraint on the subvolume registration and aids in maintaining image integrity by preventing individual subvolumes from drifting far off from their starting positions at each hierarchical level.

After registration at the last hierarchical level, the rigid-body transformations are assigned to the centers of the respective subvolumes. For every voxel in the reference image, a unique mapping transformation is determined by performing tricubic interpolation between the subvolume centers. The 3D translational component of the transformation is interpolated separately as 3 scalars, due to the independence of the translations along the 3 coordinate axes. We perform interpolation of 3D rotation in the quaternion domain, by converting the rotational matrices into quaternions (Appendix). The concept of quaternions allows a unique and complete representation of 3D rotation with elegant formulations of a range of interpolation methods. We use the equivalent of cubic interpolation for quaternions called spherical cubic interpolation or *squad* (spherical *quad*angle) as introduced by Shoemake (25). Next, using the transformation field, we resample the original PET image (22) to generate a continuous elastically transformed PET image that aligns well with the CT image.

Validation

We evaluate the accuracy of the whole-body PET/CT registration by comparing the alignment of several anatomic landmarks (3D locations within the images) as predicted by the algorithm against a reference. Because of the lack of a gold standard for this registration application (23), we assume the ability of clinical experts to locate landmarks in both CT and PET images as a suitable benchmark performance. We contend that comparing the variability in landmark matching between algorithm- and expert-defined registrations with the variability among the 3 expert-defined registrations is a reasonable way to estimate the 3D registration accuracy of the algorithm and assess whether its performance is comparable to that of the experts.

Three clinical experts, experienced in interpreting whole-body PET and CT images, were involved in the validation procedure. All experts were unaware of the identities of the subjects. Each expert was asked to identify and mark anatomic landmarks identifiable in both imaging modalities from a list of 32 well-described anatomic landmarks. Examples of anatomic landmarks are right and left lung apex, upper and lower tips of kidneys, dome of the liver, any cancerous nodule, and so forth. The experts were asked to mark the maximum possible landmarks from this list, provided they were confident of identifying a given landmark in both CT and PET images. They, on average, spent 20–30 min marking all such landmarks in a pair of PET/CT images. Three thin-plate spline-based elastic deformation fields were generated based on the homologous landmarks identified by the 3 experts, representing the respective expert-defined PET/CT elastic image registration.

Because the location of a specific landmark as marked by an expert varied slightly from expert to expert, a set of “test landmarks” was created for each case separately, by defining the location of each landmark as the centroid of the expert-defined locations for that landmark in CT. The expert-defined deformation fields were then used to determine distinct sets of homologous PET landmarks (PET₁, PET₂, and PET₃, respectively), each representing the transformed locations of the test landmarks according to the manual registration performed by one of the experts independently. The average expert-defined transformed locations (PET_{EXPERT}) were determined as the average of PET₁, PET₂, and PET₃. The

algorithm-determined transformation field was used to determine a set of landmarks in the PET image (PET_{ALGO}) representing the transformed locations of the test landmarks after the automatic elastic registration. Figure 1 graphically illustrates the concept of our validation approach.

For each case, the mean error between PET_{EXPERT} and PET_{ALGO} was evaluated to quantify the registration accuracy for that case. To further evaluate the algorithm performance in the context of interexpert variability, the 4 sets of PET points were allocated to separate groups of 3 sets each: group 1 consisted of PET_1 , PET_2 , PET_3 ; group 2 consisted of PET_1 , PET_2 , PET_{ALGO} ; group 3 consisted of PET_1 , PET_3 , PET_{ALGO} ; and group 4 consisted of PET_2 , PET_3 , PET_{ALGO} . For each group, the mean difference (Euclidean distance) in the transformed location of corresponding landmarks was obtained for all pairwise combinations of sets of PET points within that group. The mean difference for each group was determined by averaging over all cases, including only those landmarks that have been identified by all experts in a given case. Comparable mean difference values obtained for all 4 groups is an indication of good agreement between the algorithm-determined registration and the 3 expert-determined registrations. Significantly increased (or decreased) value of the mean difference in transformed locations when the algorithm replaces any expert would indicate that the algorithm-determined registration agrees less (or more) with the registration defined by that expert.

The results of the validation study were analyzed separately for the 15 cases involving images acquired on separate scanners and for the 5 cases from the combined PET/CT scanner. For the 5 combined PET/CT cases, we tabulate the mean difference values for mechanical registration against the experts before presenting similar data for the algorithm. Decrease in the variability after elastic registration would indicate the inability of combined PET/CT scanners to achieve perfect alignment and the ability of our algorithm to improve on their result.

RESULTS

Registration was performed on a Dell workstation (Xeon 2.00-GHz processor, 2.00-GB RAM) running Microsoft Windows XP Professional. For image pairs from separate

scanners, an average initial seeding of 75 mm in the axial direction was provided to compensate for different scanner coordinate systems and ensure reasonable overlap of common regions in both images. No such initial seeding was required for PET/CT from the combined scanner. No other initial seeding step was performed. All 20 image pairs registered visually correct. The average execution time for registration of a single dataset was approximately 75 min for images from the separate scanners and approximately 45 min for images from the combined scanner. The longer execution time for registration of PET/CT images from separate scanners is anticipated because of the higher degree of misalignment expected for these images as compared with the images from the combined scanner.

Figure 2 shows an example of improvement in image alignment after elastic registration as compared with only rigid-body registration for PET and CT acquired on separate scanners. Figure 3 highlights the residual misalignment in PET/CT images acquired on the combined scanner and the subsequent improvement in image alignment after registration. Figure 2 shows the ability of the registration algorithm to improve alignment of a cancerous mass as seen in CT and PET images.

The mean registration error (5.5 and 5.9 mm for images from separate scanners and combined scanner, respectively), calculated as $PET_{EXPERT} - PET_{ALGO}$, was found comparable to the mean interexpert difference in landmark identification (5.6 ± 2.4 mm and 6.6 ± 3.4 mm, respectively) calculated using corresponding PET_1 , PET_2 , and PET_3 . Statistical analysis using *t* tests did not indicate a statistically significant difference between the mean registration error and the mean interobserver error for any of the 20 cases, indicating that registration performed by the algorithm is comparable to the average expert-defined registration. To estimate the reproducibility of the algorithm-determined registration solution, the registration algorithm was implemented for a typical PET/CT pair, starting from 10 randomly generated initial misalignments (± 15 voxels for translations and $\pm 10^\circ$ for rotations). The registration error (similar to the average error reported above) for all 10 attempts was within 1-voxel range of the average error for all attempts. This indicates the robustness of the algorithm and its relative independence of the initial misalignment.

Table 1 summarizes the analysis of the interobserver variability in landmark identification averaged over the 15 cases having PET and CT from separate scanners. The results have been analyzed for the overall anatomy and then separately for the thoracic and abdominal regions of the anatomy. It can be seen from Table 1 that for a given region (overall/thoracic/abdominal), the value of the mean difference in transformed locations for any given group lies within the 95% confidence interval (CI) of the mean for the remaining 3 groups, indicating that the algorithm can replace any expert without increasing the interobserver variability in registration. On the basis of these results it can be concluded that the performance of the algorithm-determined

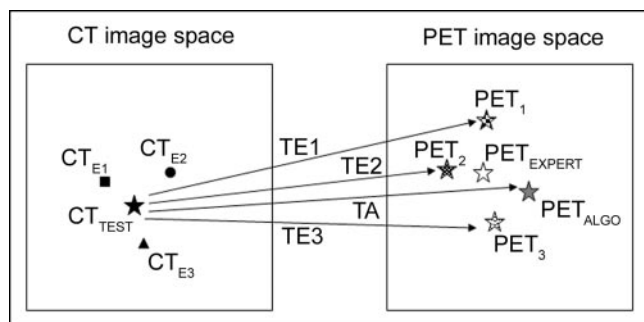


FIGURE 1. Graphic illustration of the concept of test landmarks and validation approach. TE1, TE2, TE3: Transformation fields determined independently by experts 1, 2, and 3, respectively; TA: Transformation field determined using algorithm; CT_{E1} , CT_{E2} , CT_{E3} : Location of a landmark identified in CT image space independently by experts 1, 2, and 3, respectively; CT_{TEST} : Test landmark, calculated as average of (CT_{E1} , CT_{E2} , CT_{E3}); PET_{EXPERT} is calculated as average of (PET_1 , PET_2 , PET_3).

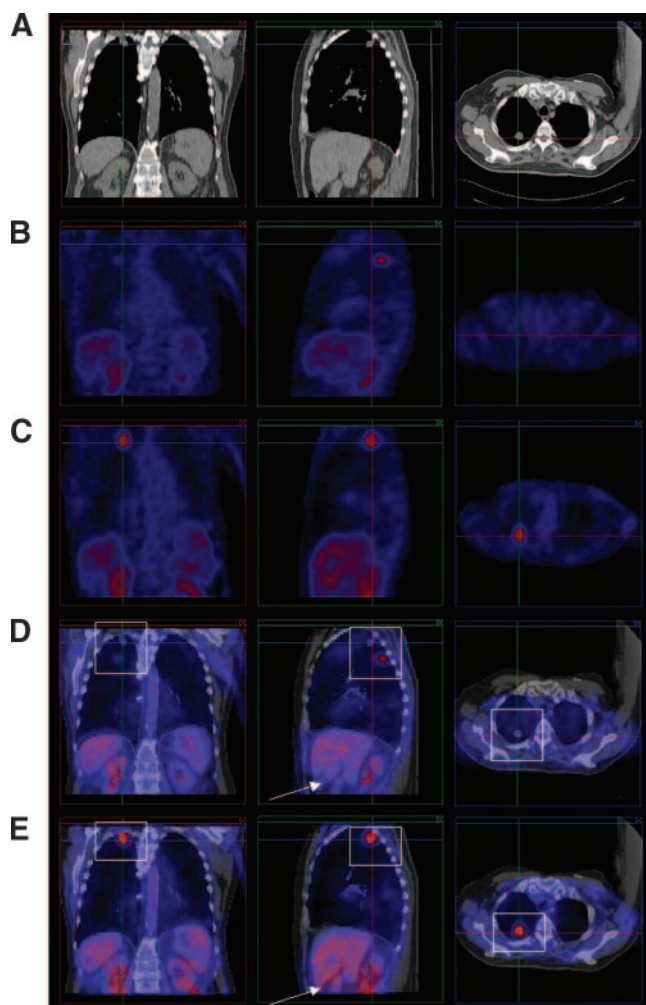


FIGURE 2. Example of registration of CT and PET images acquired from separate scanners. (A) Original CT. (B) PET after rigid-body registration. (C) PET after elastic registration. (D) PET/CT fused after rigid-body registration. (E) PET/CT fused after elastic registration. Solid rectangles highlight improvement in matching of a cancerous mass in CT and PET after elastic registration as compared with only rigid-body registration. Also note the improved matching near the liver (marked by arrows) after elastic registration as compared with rigid-body registration.

registration is comparable to all 3 expert-defined registrations.

Table 2 summarizes the interexpert variability averaged over all landmarks for the 5 cases having PET and CT images acquired using the combined PET/CT scanner. In Table 2, the original (mechanical) registration of the combined PET/CT scanner and the algorithm-determined registration are compared separately with the registration performed by the experts. A virtually unchanged mean difference value whenever the algorithm-determined registration was included in a group indicates that the algorithm performed on par with the experts' view of optimal alignment. On the other hand, a larger mean difference value, whenever the mechanical registration was included in a

group, indicates that the combined PET/CT performed slightly inferiorly compared with the experts' view of optimal alignment. Overall better "algorithm-expert" agreement (lower mean difference value) as compared with "mechanical registration-expert" agreement is evident from the statistically significant improvement (t test, $\alpha = 0.05$) in the mean difference values for groups 2–4 in Table 2 when mechanical registration was replaced with our algorithm. The difference between the algorithm and the mechanical registration is also statistically significant for registration in the thoracic region, but not so for the abdominal region, indicating that both registrations are comparable for features of the abdominal anatomy.

DISCUSSION

We have presented a new retrospective image registration algorithm capable of removing rigid (linear) as well as

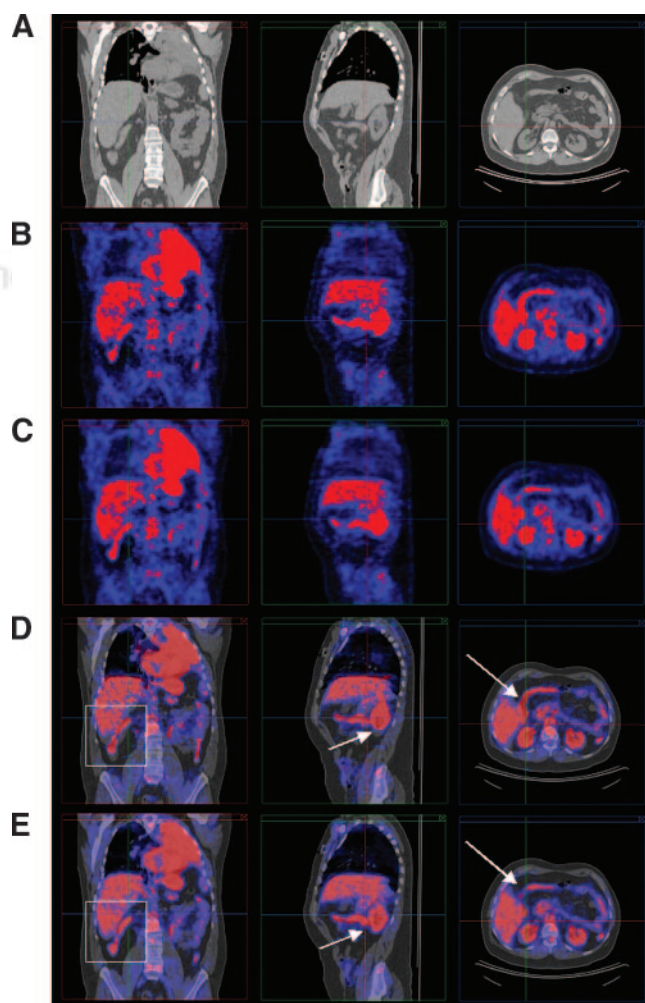


FIGURE 3. Registration of CT and PET acquired using combined PET/CT scanner. (A) Original CT. (B) Original PET. (C) PET after elastic registration. (D) Original PET/CT fused. (E) PET/CT fused after elastic registration. Rectangular box and arrows highlight improvement in matching in corresponding areas after elastic registration.

TABLE 1
Interobserver Variability in Landmark Identification (Algorithm and 3 Experts) for 15 Cases with
CT and PET Images from Separate Scanners

Anatomic region	Interobserver variability in landmark identification			
	Mean (95% CI) (mm)			
	Maximum (mm)			
	Group 1	Group 2	Group 3	Group 4
Overall	5.6 (4.9, 6.2) 11.2	5.8 (5.3, 6.5) 11.2	5.7 (5.1, 6.2) 10.9	6.0 (5.5, 6.5) 12.1
Thoracic	5.7 (5.0, 6.4) 10.9	6.2 (5.8, 6.7) 10.9	5.9 (5.3, 6.5) 10.9	6.1 (5.6, 6.7) 12.1
Abdominal	5.4 (4.2, 6.7) 11.2	5.0 (3.8, 6.1) 11.2	5.1 (3.9, 6.3) 10.7	5.3 (4.5, 6.1) 11.7

CI = confidence interval.
Group 1: PET₁, PET₂, PET₃; Group 2: PET₁, PET₂, PET_{ALGO}; Group 3: PET₁, PET₃, PET_{ALGO}; Group 4: PET₂, PET₃, PET_{ALGO}.

elastic (nonlinear) mismatch present in a pair of whole-body PET and CT images. If acquired separately, PET and CT images are misaligned because of differences in coordinate systems, body positioning, breathing protocols, and, sometimes, even couch shapes. The net misalignment from all of these factors is complex and nonlinear in nature. Our algorithm can successfully register such images. Our algorithm can also improve the registration of combined PET/CT scanners by eliminating any nonlinear residual misalignment arising from possible breathing pattern differences and interscan patient motion.

Accuracy is paramount to the success of any image registration method; therefore, we adopted a very rigorous validation approach, despite being labor intensive and time-consuming. A common problem with evaluating the performance of multimodality elastic registration is the lack of a gold standard. Expert opinion, on which often the clinical care rests, appears to be the closest substitute for a gold standard. Because experts generally differ among themselves, it is not possible to demonstrate that a new method is superior to a human expert even if that were the case. What is possible, however, is to show that the new method is at least equivalent in performance to an average human expert. Comparable interexpert and 2 experts + algorithm variabilities in Tables 1 and 2 led us to conclude that our algorithm performed as well as an average human expert and could possibly be viewed as the fourth expert. We also observed slightly higher mean difference values for images from a combined PET/CT scanner (Table 2) than those from separate scanners (Table 1). This could be attributed to low-dose noncontrast-enhanced CT images. Though none of the experts explicitly complained about this fact, lower contrast could have impacted their selection of landmarks, leading to increased variability. Another possibility is the smaller sample size (5 vs. 15 cases) used for combined-scanner images.

Previously reported elastic registration methods for PET/CT have been validated either only qualitatively or

with not as much rigor. Tai et al. (7) used the number of mismatched voxels as a measure for registration accuracy. Slomka et al. (8) used indirect means such as reproducibility tests, algorithm convergence, and qualitative visual assessment for validation of their algorithm. To the best of our knowledge, only Mattes et al. (23) have reported registration accuracy in terms of physical dimensions for whole-body PET/CT registration. However, they evaluated only the in-plane translational accuracy of the registration by using several reformatted sagittal, coronal, and axial images and reported 0- to 6-mm error range for the thoracic region versus 6- to 11-mm error range for the abdominal region. The mean registration error and other results presented in Tables 1 and 2 from our comprehensive validation approach compare favorably with the registration accuracy reported by Mattes et al. (23).

Our reported execution time of 45–75 min compares favorably with approximately 100 min for the multiresolution free-form deformation (FFD)-based approach reported (23) for similar but smaller images (in-plane voxel count about a quarter of our images). This is because an image subdivision-based approach (like ours) is computationally simpler (the transformation mode remains rigid locally) as compared with the FFD-based approach, making our algorithm more efficient to compute and, hence, faster without compromising accuracy. Independent of the current work, we have developed a new hardware platform called FAIR (fast automatic image registration) for accelerated execution of MI/NMI-based image registration (12,26,27). Further reduction in the reported execution time is possible when we implement our algorithm on the FAIR platform.

The question of whether to use emission or transmission PET often arises in PET/CT registration. The transmission scan, for being similar to CT, has been successfully used by many investigators (7,23). The emission scan is substituted for the transmission scan after registration in these methods. Although inadequate for clinical decision-making, the non-

TABLE 2
Interobserver Variability in Landmark Identification: Comparison Between Algorithm-Based and Scanner-Based Registration for 5 Cases with CT and PET Images from Combined Scanner

		Interobserver variability in landmark identification Mean (95% CI) (mm) Maximum (mm)		P value
Anatomic region		Scanner (mechanical registration)	Algorithm (elastic registration)	
Group 1	Overall	6.6 (5.9, 7.2) 12.3	6.6 (5.9, 7.2) 12.3	—
	Thoracic	7.2 (6.6, 7.9) 12.3	7.2 (6.6, 7.9) 12.3	—
	Abdominal	5.5 (4.5, 6.5) 11.6	5.5 (4.5, 6.5) 11.6	—
Group 2	Overall	7.0 (6.4, 7.7) 14.3	6.0 (5.5, 6.6) 14.1	<0.05
	Thoracic	8.1 (7.4, 8.8) 14.3	6.8 (6.2, 7.4) 11.9	<0.05
	Abdominal	5.4 (4.4, 6.4) 12.9	4.8 (3.9, 5.8) 14.1	NS
Group 3	Overall	7.2 (6.6, 7.9) 12.9	6.1 (5.5, 6.6) 12.3	<0.05
	Thoracic	8.3 (7.5, 9.1) 12.9	6.8 (6.1, 7.5) 12.3	<0.05
	Abdominal	5.5 (4.5, 6.5) 11.6	4.8 (4.1, 5.7) 11.6	NS
Group 4	Overall	8.2 (7.5, 8.9) 13.1	6.5 (5.9, 7.1) 11.7	<0.05
	Thoracic	9.5 (8.6, 10.4) 12.5	7.5 (6.7, 8.2) 11.7	<0.05
	Abdominal	6.2 (5.0, 7.5) 13.1	5.2 (4.0, 6.4) 10.9	NS

NS = not significant.

Group 1: PET₁, PET₂, PET₃; Group 2: PET₁, PET₂, PET_{SCANNER} or PET_{ALGO}; Group 3: PET₁, PET₃, PET_{SCANNER} or PET_{ALGO}; Group 4: PET₂, PET₃, PET_{SCANNER} or PET_{ALGO}.

specific uptake of the PET tracer by different organs in emission scans often permits using them directly in image registration. In a comparative study, Skalski et al. (28) reported achieving higher accuracy with the transmission scan, but perhaps the optimal approach is to use a weighted sum of the 2 images, as suggested by Slomka et al. (8). In general, when working with separately acquired CT and PET and using the transmission scan for registration, any movement between the transmission and emission scans cannot be corrected. Transmission images, which offer poorer contrast resolution in the abdominal region, may also lower registration accuracy in the abdominal region compared with that in the thoracic region, as Mattes et al. (23) report. Indeed, no such debate exists for combined PET/CT scans because the CT itself is used for attenuation correction and a transmission scan does not exist. Thus, any registration must use emission PET. The accuracy of our method validates the use of the emission scan for PET/CT registration. Using a misregistered CT scan for attenuation correction in PET in com-

bined PET/CT can itself be a source of misalignment and uptake errors (29). Further improvement of whole-body PET/CT image registration by using motion-corrected CT images for PET attenuation correction constitutes a future direction of our research.

Software image registration is flexible, powerful, and versatile (30) and we contend that it will continue to be needed despite the increasing deployment of combined PET/CT scanners. Combined PET/CT scanners neutralize rigid misalignment but not nonrigid misalignment. For applications demanding high registration accuracy, such as intensity-modulated radiotherapy, our method can be used to refine combined PET/CT images. Indeed, our method can be used in facilities lacking a combined scanner and for retrospective registration of an existing diagnostic CT scan with a combined PET/CT scan. Additionally, serial comparison of combined whole-body PET/CT images acquired at different times can only be accomplished through an algorithmic method such as ours.

CONCLUSION

We have presented a new, efficient, and fully automatic (free of manual steps) voxel-based algorithm for elastic image registration of whole-body PET and CT images. This algorithm can register PET/CT images from separate scanners with accuracy on par with manual elastic registration performed by human experts using up to 32 anatomic landmarks. More importantly, the algorithm is also capable of enhancing the alignment of PET/CT scans obtained from a combined scanner. The combined PET/CT scans are known to exhibit nonrigid misalignment artifacts due to differences in breathing protocols during individual scans. Such artifacts are a problem if the resulting images are to be used for highly conformal radiotherapies and image-guided interventions. Consequently, even in the age of combined scanners, software elastic registration methods are expected to play a significant role as only they can correct for nonlinear mismatches and permit serial comparison. The success of a software registration method will depend on both accuracy and speed. The proposed method is accurate and relatively fast and can be further accelerated through hardware-based implementation.

APPENDIX

A quaternion is an extension of a complex number and is usually expressed as:

$$Q = w + xi + yj + zk;$$

$$i^2 = j^2 = k^2 = -1, ij = k, ji = -k. \quad \text{Eq. 1A}$$

An alternative representation of a quaternion as a combination of a scalar and a vector in 3D space is:

$$Q = [w, v]; w \in \mathbb{R}, v = [x, y, z] \in \mathbb{R}^3. \quad \text{Eq. 2A}$$

Quaternions are useful for representation of 3D rotational pose. A 3D rotation θ about an axis given by a unit vector $a = [a_x, a_y, a_z]$ can be represented using a unit quaternion (magnitude unity) as follows:

$$q = \left[\cos\left(\frac{\theta}{2}\right), a \cdot \sin\left(\frac{\theta}{2}\right) \right]. \quad \text{Eq. 3A}$$

A 1:1 relationship also exists between a unit quaternion representing a 3D rotation and a 3×3 real orthogonal rotation matrix corresponding to a given Euler angle triplet:

$$M = \begin{bmatrix} 1 - 2y^2 - 2z^2 & 2xy + 2wz & 2xz - 2wy \\ 2xy - 2wz & 1 - 2x^2 - 2z^2 & 2yz + 2wx \\ 2xz + 2wy & 2yz - 2wx & 1 - 2x^2 - 2y^2 \end{bmatrix}$$

$$\Leftrightarrow q = [w, (x, y, z)]. \quad \text{Eq. 4A}$$

Quaternion interpolation (for uniquely interpolating 3D rotational pose) is performed on the surface of a 4-dimensional (4D) hypersphere. The equivalent of linear interpolation for quaternions on a 4D hypersphere is called “spherical linear interpolation” or *slerp*. For unit quaternions q_0 ,

q_1 and interpolation fraction $t \in [0,1]$ the spherical linear interpolation curve is defined as:

$$\text{slerp}(q_0, q_1, t) = \frac{\sin((1-t)\theta)}{\sin\theta} q_0 + \frac{\sin(t\theta)}{\sin\theta} q_1,$$

where $\theta = \cos^{-1}(q_0 \cdot q_1)$. Eq. 5A

The higher order spherical cubic interpolation or *squad* (spherical and *quad*angle) for quaternions was used in our work. For unit quaternions q_i, q_{i+1} and interpolation fraction $t \in [0,1]$, the following interpolation function was used:

$$\text{squad}(q_i, a_i, a_{i+1}, q_{i+1}, t) = \text{slerp}(\text{slerp}(q_i, q_{i+1}, t), \text{slerp}(a_i, a_{i+1}, t), 2t(1-t)); t \in [0,1].$$

$$a_i = q_i \exp\left(-\left(\frac{\ln(q_i^{-1} \cdot q_{i+1}) + \ln(q_i^{-1} \cdot q_{i-1})}{4}\right)\right). \quad \text{Eq. 6A}$$

ACKNOWLEDGMENT

This project is supported by the Whitaker Foundation research grant RG-01-0071.

REFERENCES

1. Kapoor V, McCook BM, Torok FS. An introduction to PET-CT imaging. *Radiographics*. 2004;24:523–543.
2. Wahl RL, Quint LE, Greenough RL, Meyer CR, White RI, Orringer MB. Staging of mediastinal non-small cell lung cancer with FDG PET, CT, and fusion images: preliminary prospective evaluation. *Radiology*. 1994;191:371–377.
3. Townsend DW, Carney JP, Yap JT, Hall NC. PET/CT today and tomorrow. *J Nucl Med*. 2004;45(suppl 1):4S–14S.
4. Yap JT, Carney JP, Hall NC, Townsend DW. Image-guided cancer therapy using PET/CT. *Cancer J*. 2004;10:221–233.
5. Lavelly WC, Scarfone C, Cevikalp H, et al. Phantom validation of coregistration of PET and CT for image-guided radiotherapy. *Med Phys*. 2004;31:1083–1092.
6. Cohade C, Wahl RL. Applications of positron emission tomography/computed tomography image fusion in clinical positron emission tomography: clinical use, interpretation methods, diagnostic improvements. *Semin Nucl Med*. 2003;33:228–237.
7. Tai Y-C, Lin KP, Hoh CK, Huang SCH, Hoffman EJ. Utilization of 3-D elastic transformation in the registration of chest x-ray CT and whole body PET. *IEEE Trans Nucl Sci*. 1997;44:1606–1612.
8. Slomka PJ, Dey D, Przetak C, Aladi UE, Baum RP. Automated 3-dimensional registration of stand-alone ^{18}F -FDG whole-body PET with CT. *J Nucl Med*. 2003;44:1156–1167.
9. Beyer T, Antoch G, Blodgett T, Freudenberg LF, Akhurst T, Mueller S. Dual-modality PET/CT imaging: the effect of respiratory motion on combined image quality in clinical oncology. *Eur J Nucl Med Mol Imaging*. 2003;30:588–596.
10. Goerres GW, Kamel E, Seifert B, et al. Accuracy of image coregistration of pulmonary lesions in patients with non-small cell lung cancer using an integrated PET/CT system. *J Nucl Med*. 2002;43:1469–1475.
11. de Juan R, Seifert B, Berthold T, von Schulthess GK, Goerres GW. Clinical evaluation of a breathing protocol for PET/CT. *Eur Radiol*. 2004;14:1118–1123.
12. Shekhar R, Zagrodsky V, Castro-Pareja CR, Walimbe V, Jagadeesh JM. High-speed registration of three- and four-dimensional medical images by using voxel similarity. *Radiographics*. 2003;23:1673–1681.
13. Maes F, Collignon A, Vandermeulen D, Marchal G, Suetens P. Multimodality image registration by maximization of mutual information. *IEEE Trans Med Imaging*. 1997;16:187–198.
14. Wells WM 3rd, Viola P, Atsumi H, Nakajima S, Kikinis R. Multi-modal volume registration by maximization of mutual information. *Med Image Anal*. 1996;1:35–51.
15. Pluim JP, Maintz JB, Viergever MA. Mutual-information-based registration of medical images: a survey. *IEEE Trans Med Imaging*. 2003;22:986–1004.
16. Studholme C, Hill DLG, Hawkes DJ. An overlap invariant entropy measure of 3D medical image alignment. *Pattern Recognit*. 1999;32:71–86.
17. Carrillo A, Duerk JL, Lewin JS, Wilson DL. Semiautomatic 3-D image registration as applied to interventional MRI liver cancer treatment. *IEEE Trans Med Imaging*. 2000;19:175–185.

18. Studholme C, Hill DL, Hawkes DJ. Automated three-dimensional registration of magnetic resonance and positron emission tomography brain images by multiresolution optimization of voxel similarity measures. *Med Phys*. 1997;24:25–35.
19. Meyer CR, Boes JL, Kim B, et al. Semiautomatic registration of volumetric ultrasound scans. *Ultrasound Med Biol*. 1999;25:339–347.
20. Shekhar R, Zagrodsky V. Mutual information-based rigid and nonrigid registration of ultrasound volumes. *IEEE Trans Med Imaging*. 2002;21:9–22.
21. Walimbe V, Zagrodsky V, Raja S, et al. Mutual information-based multimodality registration of cardiac ultrasound and SPECT images: a preliminary investigation. *Int J Cardiovasc Imaging*. 2003;19:483–494.
22. Walimbe V, Zagrodsky V, Raja S, Bybel B, Kanvinde M, Shekhar R. Elastic registration of three-dimensional whole body CT and PET images by quaternion-based interpolation of multiple piecewise linear rigid-body registrations. *Proc SPIE*. 2004;5370:1191–1228.
23. Mattes D, Haynor DR, Vesselle H, Lewellen TK, Eubank W. PET-CT image registration in the chest using free-form deformations. *IEEE Trans Med Imaging*. 2003;22:120–128.
24. Izenman AJ. Recent developments in nonparametric density estimation. *J Am Stat Assoc*. 1991;86:205–224.
25. Shoemake K. Quaternion calculus and fast animation. *SIGGRAPH Course Notes*. 1987;10:101–121.
26. Castro-Pareja CR, Jagadeesh JM, Shekhar R. FAIR: a hardware architecture for real-time 3-D image registration. *IEEE Trans Inf Technol Biomed*. 2003;7:426–434.
27. Castro-Pareja CR, Shekhar R. Hardware acceleration of mutual information-based 3D image registration. *J Imaging Sci Technol*. 2005;49:105–113.
28. Skalski J, Wahl RL, Meyer CR. Comparison of mutual information-based warping accuracy for fusing body CT and PET by 2 methods: CT mapped onto PET emission scan versus CT mapped onto PET transmission scan. *J Nucl Med*. 2002;43:1184–1187.
29. Nakamoto Y, Chin BB, Cohade C, Osman M, Tatsumi M, Wahl RL. PET/CT: artifacts caused by bowel motion. *Nucl Med Commun*. 2004;25:221–225.
30. Slomka PJ. Software approach to merging molecular with anatomic information. *J Nucl Med*. 2004;45(suppl 1):36S–45S.





The Journal of
NUCLEAR MEDICINE

Automated 3-Dimensional Elastic Registration of Whole-Body PET and CT from Separate or Combined Scanners

Raj Shekhar, Vivek Walimbe, Shanker Raja, Vladimir Zagrotsky, Mangesh Kanvinde, Guiyun Wu and Bohdan Bybel

J Nucl Med. 2005;46:1488-1496.


This article and updated information are available at:
<http://jnm.snmjournals.org/content/46/9/1488>

Information about reproducing figures, tables, or other portions of this article can be found online at:
<http://jnm.snmjournals.org/site/misc/permission.xhtml>

Information about subscriptions to JNM can be found at:
<http://jnm.snmjournals.org/site/subscriptions/online.xhtml>

The Journal of Nuclear Medicine is published monthly.
SNMMI | Society of Nuclear Medicine and Molecular Imaging
1850 Samuel Morse Drive, Reston, VA 20190.
(Print ISSN: 0161-5505, Online ISSN: 2159-662X)

© Copyright 2005 SNMMI; all rights reserved.

 SOCIETY OF
NUCLEAR MEDICINE
AND MOLECULAR IMAGING